Iron-ion–implantation effects in MgO crystals

A. Perez
Département de Physique des Matériaux, Université Claude Bernard Lyon I, F-69622 Villeurbanne, France

G. Marest
Institut de Physique Nucléaire, Université Claude Bernard Lyon I, F-69622 Villeurbanne, France

B. D. Sawicka
Institute of Nuclear Physics, Cracow, Poland

J. A. Sawicki
Institute of Physics, Jagiellonian University, Cracow, Poland

T. Tyliszczak
Institute of Physics, Technical University, Cracow, Poland

(Received 17 February 1983)

Magnesium oxide crystals implanted with $^{57}Fe^+$ ions at doses ranging from 10^{15} to 10^{17} ions/cm^2 (ion energy 70, 100, and 150 keV) were studied with the conversion-electron Mössbauer-spectroscopy technique. Supplementary data were obtained using the techniques of Rutherford backscattering and channeling of α particles, optical absorption, electron microscopy, and electrical conductivity. It was found that implantation introduces iron in MgO in three charge states: Fe^{2+}, Fe^{3+}, and metallic precipitates (Fe^0) with the dominant role of Fe^{3+} at low doses, Fe^{2+} at medium doses, and metallic iron clusters at the highest doses. The phase created in a medium range of doses can be compared with the magnesio-wüstite solid solution. The isochronal thermal annealings in air at temperatures between 300 and 700 °C gradually cause the oxidation and the nucleation of highly dispersed spinel-like clusters and then, at about 800–900 °C, the growth of magnesioferrite particles. In contrast, the heat treatment in vacuum converts all iron into well-diluted Fe^{2+} in MgO phase. The nature of point defects and their role in annealing processes are discussed on the basis of the optical absorption data. A good correspondence between the results of Mössbauer and channeling data is indicated. The effect of the insulator-conductor transition occurring under iron-ion implantation in MgO and observed by electrical conductivity measurements is explained in terms of the atomistic properties of implanted crystals under study.

I. INTRODUCTION

Heavy-ion bombardment of ionic crystals causes very complex structural changes and chemical effects, the knowledge of which is still limited until now.[1] The solid phase which is created as a result of high-density cascades can incorporate implanted impurities in various charge states, which in turn can associate with various lattice defects, thus creating a multitude of metastable impurity-defect structures. Thermal annealing usually removes a great deal of lattice damage and leads via nucleation and diffusion to the growth of different precipitates of various equilibrium systems, which can be therefore predicted (and are sometimes well known) on the basis of classical phase diagrams. Therefore, when describing the nature of the as-implanted phases, the systematic investigations of the annealing behavior of implanted crystals are very helpful. A characterization of metastable phases created by a high-dose ($\geq 10^{16}$ ions/cm^2) implantation of metallic ions into a refractory oxide MgO has been a subject of particular interest for several years.[2–5] The results obtained until now show that the nature of precipitates in MgO depends strongly on the kind of ions used[2]: (i) Alkali-metal ions (Li, Na, K, Rb) tended to form small metallic precipitates, (ii) indium and gold were used to form binary alloys with magnesium, and (iii) iron was found to oxidize and at elevated temperatures to form spinel ferrite particles.[3,4]

Various experimental methods employed thus far in the investigation of iron implantation in MgO included conversion-electron Mössbauer spectroscopy (CEMS), optical absorption (OA), Rutherford backscattering (RBS) and channeling techniques,[3] transmission electron microscopy[4] (TEM), and electrical conductivity measurements.[5] In order to characterize the investigated structures and processes, we performed systematic CEMS measurements which concentrated on two problems: (i) the dose dependence of Mössbauer spectra (from 10^{15} to 10^{17} ions/cm^2) and (ii) the isochronal thermal annealing behavior (up to 1000 °C); these studies are the subject of this paper. Systematic complementary measurements by means of OA, RBS, and channeling methods are also reported.

The study of iron-ion implantation in MgO presents for

TABLE I. Mössbauer parameters of various components present in as-implanted Fe-MgO samples (Fe^{3+}, $Fe^{2+}{}_{I}$, $Fe^{2+}{}_{II}$, and metallic iron Fe^{0}), obtained by computer fitting of the spectra. E is the energy of the implanted $^{57}Fe^{+}$ ions, $\bar{x}$ is the iron concentration in the implanted zone, T is the temperature of the Mössbauer measurement, Δ_{IS} is the isomer shift, Δ_{QS} is the quadrupole splitting, W is the linewidth, and R is the relative area.

					Fe^{3+}			
No.	Dose (ions/cm^2)	E (keV)	$\bar{x}$ (%)	T (K)	Δ_{IS} (mm/s)	Δ_{QS} (mm/s)	W (mm/s)	R (%)
1	10^{15}	70	0.3	293				
2	3×10^{15}	100	0.6	293	0.44	0.65	0.52	62.0
3	5×10^{15}	70	1.5	293	0.38	0.69	0.56	33.1
4	7×10^{15}	70	2.1	293	0.37	0.58	0.78	33.3
5	10^{16}	70	3.0	293	0.38	0.63	0.34	11.9
6	2×10^{16}	100	4.0	293	0.51	0.56	0.30	8.9
7[a]	2×10^{16}	100	4.0	293	0.37	0.65	0.64	34.3
	2×10^{16}	100	4.0	77	0.53	0.74	1.28	32.1
8	3×10^{16}	100	6.0	293	0.39	0.64	0.40	0.6
	3×10^{16}	100	6.0	77	0.34	0.74	0.30	2.1
9	4×10^{16}	100	8.0	293	0.36	0.66	0.46	7.6
10	6×10^{16}	100	12.0	77	0.53	0.68	0.54	6.3
11	5×10^{16}	70	15.0	293	0.41	0.68	0.52	2.5
12	8×10^{16}	100	16.0	293	0.29	0.69	0.90	38.2
	8×10^{16}	100	16.0	77	0.30	0.65	0.94	39.0

many reasons a special scientific and practical interest. For instance, it is well known that the presence of iron considerably influences the hardness as well as electrical and thermodynamical properties of refractory oxides and ceramics. Numerous studies of valence states and iron aggregation processes in MgO have been thus far performed for samples fabricated by means of various conventional thermochemical methods (i.e., a prolonged heating and cooling at a low rate). These studies were recently concluded by Weeks *et al.*[6] and Goudrin *et al.*[7,8] One can find in the literature an impressive number of references dealing with a nonimplanted Fe-MgO system. References 9–19 (quoted in chronological order) are those which were useful in analyzing our data for MgO crystals doped with iron by means of the ion-implantation technique.

II. SAMPLE PREPARATION AND THERMAL TREATMENT

Samples were prepared by isotope separator implantation of $^{57}Fe^{+}$ ions into targets ($20\times10\times0.5$ mm^3) cleaved from a "Spicer" single-crystal block. The concentrations of intrinsic impurities in the crystal as estimated by the manufacturer are (in ppm) Al (30–40), Ca (20–30), Si (15–30), Fe (2–10), Zn (2–10), and other impurities (less than 40 ppm in total). All the implantations were carried out at room temperature, in a vacuum of about 10^{-6} Torr. Isotope separators at the Institute of Nuclear Physics in Cracow (70 keV) and Lyon (100 and 150 keV) were used. The current density was low (~1–3 μA cm^{-2}) in order to restrict thermal effects during implantation. The ion beam scanning was used in order to assure a homogeneous implantation of the whole implanted surface of the samples. Various doses of Fe^{+} ions were implanted in the range from 10^{15} to 10^{17} ions/cm^2. For both CEMS and RBS measurements the samples implanted with $^{57}Fe^{+}$ ions were mostly used, and various characteristics of these samples are collected in Table I. For optical measurements a series of samples implanted with $^{56}Fe^{+}$ ions was prepared (energy 100 keV, doses from 10^{15} to 10^{17} ions/cm^2, as indicated in Fig. 4).

The isochronal thermal treatment was performed for selected samples from 300 to 1000 °C, in 100 °C steps, for 30 min at each temperature. Sample no. 5 was annealed in a vacuum of 10^{-5} Torr; other samples, numbered 6, 9, and 10 in Table I, were annealed in air. After each annealing step the sample was quenched to room temperature.

III. RBS AND CHANNELING MEASUREMENTS

The depth profile of implanted ions was measured by Rutherford backscattering of 1.6- and 2-MeV α particles using a Van de Graaff accelerator. For chosen samples, in order to get a better depth resolution, measurements were performed at oblique incidence (70°, 2-MeV α particles). The average atomic concentration $\bar{x}$ of Fe in implanted layers (in percentage of Fe per Mg) were calculated assuming a Gaussian distribution of ranges and using the experimental width ($2\Delta R_p$) values equal to 40, 60, and 77 nm, respectively, for 70-, 100-, and 150-keV ions. The experimental mean ranges R were found to agree well with the projected ranges R_p calculated using LSS theory (see tables of Dearnaley *et al.*[20]). The experimental values for range straggling are, however, about 2 times larger than the corresponding theoretical ΔR_p values.

The Rutherford backscattering measurements allowed us to follow the depth distribution of iron atoms in a function of the annealing temperature. The RBS spectra for the MgO sample implanted with a dose of 2×10^{16} of 150-keV $^{56}Fe^{+}$ ions/cm^2, measured after several annealing steps (annealing in air), are presented in Fig. 1. As seen, the primary implantation profile is preserved up to 600 °C. Upon the heat treatment at higher temperatures one notices a gradual migration of iron into the crystal, which also causes a gradual decrease in the average iron concentration. For instance, the RBS spectrum taken after the

TABLE I. (*Continued.*)

Fe_I^{2+}				Fe_{II}^{2+}				Fe^0		
Δ_{IS} (mm/s)	Δ_{QS} (mm/s)	W (mm/s)	R (%)	Δ_{IS} (mm/s)	Δ_{QS} (mm/s)	W (mm/s)	R (%)	Δ_{IS} (mm/s)	W (mm/s)	R (%)
1.07	0.93	0.78	30.0	1.05	2.16	0.52	3.7	0.01	0.52	4.3
0.99	1.06	0.64	46.9	0.95	2.22	0.56	17.3	−0.03	0.36	1.4
0.99	0.94	0.62	40.0	1.02	2.17	0.68	24.0	0.01	0.52	3.7
0.97	1.05	0.74	53.5	0.93	2.29	0.70	31.3	−0.10	0.30	3.2
1.02	0.76	0.54	61.5	0.91	2.03	0.61	28.2	−0.03	0.36	1.2
1.15	0.94	0.70	34.5	0.95	2.28	0.58	16.2	0.01	0.70	15.0
1.17	1.12	1.20	35.2	0.97	2.34	0.64	7.2	−0.01	1.24	25.4
0.95	1.01	0.56	51.7	0.82	2.17	0.58	41.9	0.00	0.35	5.8
1.14	1.26	0.60	46.0	1.04	2.36	0.58	46.7	0.07	0.30	5.2
1.06	0.88	0.64	56.6	0.89	2.12	0.58	23.3	0.01	0.56	12.5
1.12	1.30	1.18	37.2	0.99	2.46	1.04	34.9	0.02	0.92	21.6
1.08	0.96	0.66	51.4	0.90	2.17	0.64	28.9	0.01	0.62	17.2
0.94	1.29	0.80	32.2	0.83	2.32	0.62	14.2	−0.09	0.60	15.4
1.08	1.43	0.90	36.0	0.97	2.48	0.48	10.0	−0.05	0.48	14.0

[a]Powder sample

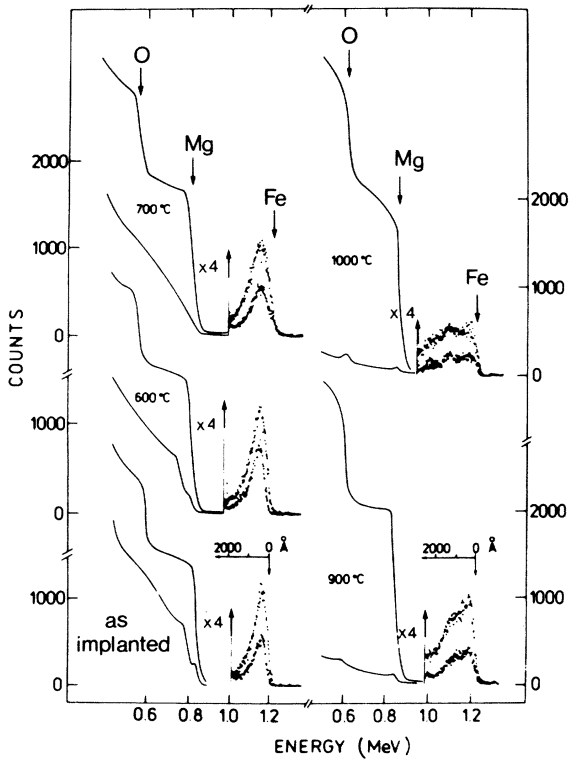

FIG. 1. Rutherford backscattering spectra for a MgO crystal implanted with 150-keV $^{56}Fe^+$ ions at the dose of 2×10^{16} ions/cm^2, measured with 1.6-MeV α particles. Solid lines represent the backscattering spectra for the MgO matrix and dotted lines present the distribution of iron (multiplied by a factor of 4). The bottom spectrum is for the as-implanted sample, others for the sample after consecutive annealing performed for 30 min in air, and at increasing temperatures. The upper line in each case is a "random" spectrum, and the lower is a channeled spectrum in the [100] direction.

annealing at 1000 °C shows iron atoms to be distributed almost uniformly in the depth of about 200 nm, which corresponds to the average concentration of $\bar{x}\simeq1.2\%$. This can be compared with the data for the as-implanted sample: $2\Delta R_p=77$ nm and $\bar{x}=3\%$. Our RBS measurements indicate that the annealing at 1000 °C causes the intensive diffusion of iron into the bulk of the crystal, with all the iron atoms remaining in the sample. This is in contrast with the case of high-dose implantation for which a different behavior is observed: The RBS data for sample no. 10 (6×10^{16} ions/cm^2), after the last annealing step (1000 °C, in air), indicate that most of the iron has diffused towards the surface of the crystal. The low-energy electron-induced x-ray spectrometry technique showed that this surface layer consists of iron oxides.[21]

Rutherford backscattering measurements performed in a channeling position allowed us to obtain detailed information concerning the degree of disorder in the magnesium sublattice, the arrangement of implanted iron ions, and the corresponding changes upon the sample annealing. The backscattering spectra and the minimum backscattering yields for Fe and Mg were measured in the [100] and [110] directions, after each annealing step. As an example, the results of the scanning around the [100] channel are plotted in Fig. 2. The corresponding minimum yields for both channels are reported in Fig. 3. The channeling measurements indicate a substantial rearrangement of Mg and Fe atoms in the cationic sublattice of MgO at temperatures between 600 and 1000 °C. The minimum yield χ_{min} for the Mg sublattice in the as-implanted sample is about 0.4 and 0.35, in the [100] and [110] directions, respectively, which indicates a high degree of disorder in the Mg sublattice (for the virgin MgO sample, $\chi_{min}\simeq0.03$). Heating of the sample at temperatures above 600 °C causes a gradual ordering of the Mg sublattice due to a redistribution of displaced Mg atoms in the cationic sublattice; after annealing at 900 and 1000 °C, χ_{min} approaches the

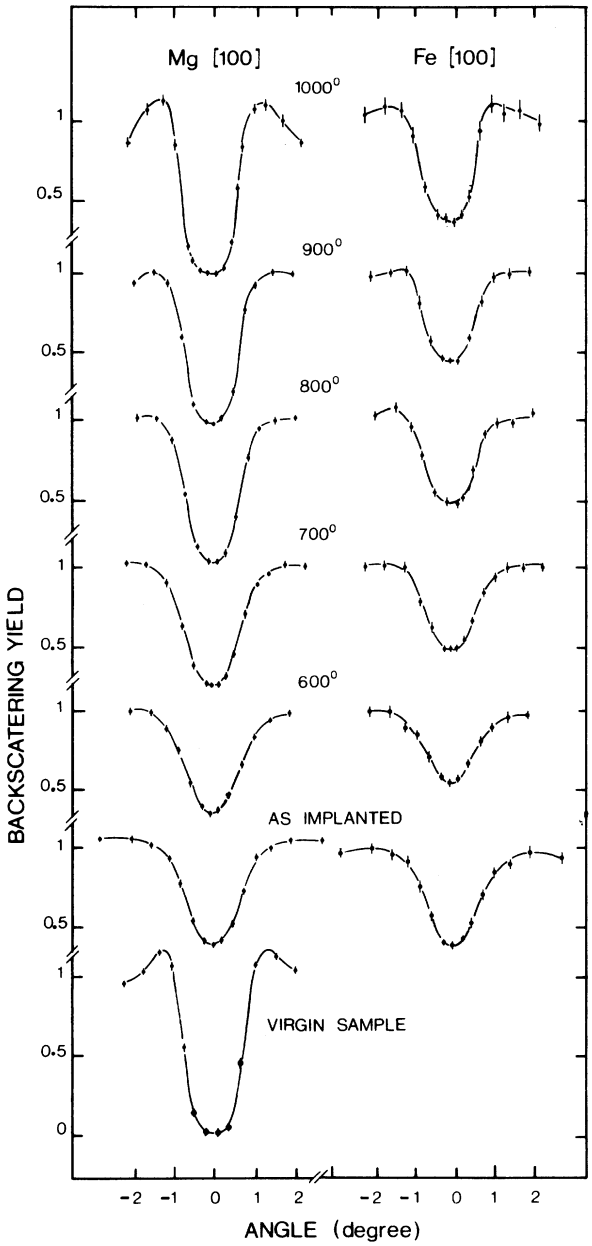

FIG. 2. Angular yield curves for the [100] channel (sample as in Fig. 1) for the nonannealed sample and for the sample annealed in air at different temperatures, as indicated. Bottom curve is for the virgin sample.

value of about 0.05. The disorder measured for iron atoms ($\chi_{min} \simeq 0.44$ and 0.54 for the [100] and [110] channels, respectively, for the nonannealed sample) increases after the first step of annealing (600 °C) and only after the 700 °C annealing the ordering effects start to be observed. However, the ordering does not proceed smoothly with the temperature; at 800 °C an increase is observed in the evolution of the minimum yields for both [100] and [110] directions and the decrease restarts at still higher temperatures (Fig. 3). After annealing at 900 and 1000 °C about 60% of iron was found at substitutional positions, and 40% at interstitial positions in MgO lattice. This result is consistent with the creation of spinel-like clusters within the MgO

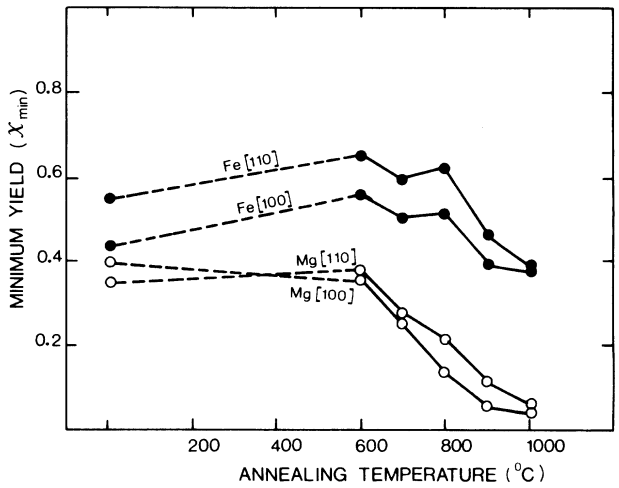

FIG. 3. Channeling measurements in the [100] and [110] directions in the MgO crystal (sample as in Figs. 1 and 2), presenting the minimum yields in a function of annealing temperature.

matrix; this will be discussed later together with the Mössbauer data. Scanning around both [100] (Fig. 2) and [110] channels indicates that channels measured at both Fe and Mg sublattices have widths similar to each other and that no significant change occurs after consecutive annealing steps.

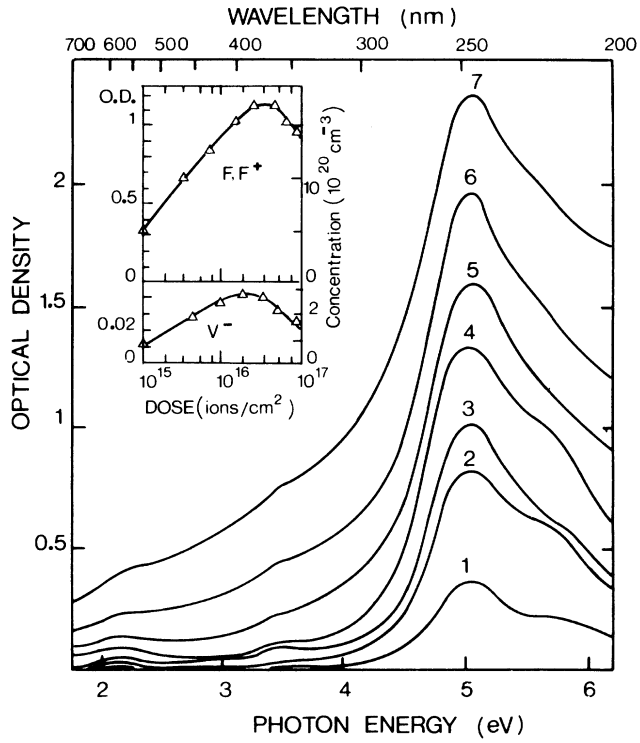

FIG. 4. Optical absorption spectra for MgO crystals implanted with 100-keV $^{56}Fe^+$ ions and the following doses: (1) 10^{15} ions/cm^2, (2) 5×10^{15}, (3) 10^{16}, (4) 2×10^{16}, (5) 4×10^{16}, (6) 6×10^{16}, (7) 8×10^{16}. The inset shows the F-type and V-type center growth curves.

IV. OPTICAL ABSORPTION MEASUREMENTS

The optical absorption spectra were recorded in the wavelength range from 200 to 1000 nm using a Cary 17 double beam spectrophotometer. The unimplanted part of the sample always served as a reference. The variation of the spectra with the ion dose, for doses between 10^{15} and 8×10^{16} ions/cm^2, is presented in Fig. 4. The spectra measured after subsequent isochronal heatings for two samples (2×10^{16} and 8×10^{16} ions/cm^2) are shown in Fig. 5.

The predominant absorption band observed in all samples at 5 eV corresponds to the overlapping bands due to F and F^+ centers. Other observed bands less intensive can be associated with, respectively, anionic vacancies[14] (5.7 eV), pairs of F centers in nearest-neighbor sites in anionic sublattice along [110] directions[22] (3.42 eV), and V-type centers in the cationic sublattice[22] (2.3-eV band). The concentrations of F-, F^+-, and V-type centers increase with the increase in the ion dose and, as shown in the inset in Fig. 4, reach the saturation for a dose of about 3×10^{16} ions/cm^2, at the following values of concentrations: 2×10^{21} cm^{-3} for F-type centers and 3×10^{20} cm^{-3} for V-type centers. Optical measurements indicate that F_2 and V-type defects anneal at temperatures below 600 °C, while the F and F^+ defects anneal mostly at temperatures between 600 and 700 °C. After annealing at 700 °C an absorption band located near 4.3 eV appears, which is a monitor for Fe^{3+} in MgO. This band was ascribed by us, according to its identification in Ref. 14, to a complex of a substitutional iron coupled to an interstitial oxygen ($Fe^{3+}O_i^{2-}$).[14] This band increases its intensity after higher-temperature annealings and reaches its maximum after the sample annealing at about 900 °C. Using the value of the oscillator strength for the 4.3-eV band, as given in Ref. 15, we estimated the number of the ($Fe^{3+}O_i^{2-}$) complexes. For the annealed samples, this number is about $(2–2.5)\times10^{16}$ cm^{-2}, both for low-dose and high-dose implanted samples. Notice that the number of the ($Fe^{3+}O_i^{2-}$) complexes formed after the sample annealing achieves the saturation and that for the samples up to the dose of 2×10^{16} ions/cm^2, all iron after annealing seems to be in a form of such complexes. The Fe^{2+} is known to have an absorption band in the near-ir region (between 1 and 1.7 eV), but it could not be detected in our measurements because of a very small oscillator strength for this band.[15] Also small metallic aggregates, if present, could not be observed directly. Such precipitates embedded in matrices of insulators are known to exhibit a broad absorption band due to a plasma resonance of free electrons. The position of this band can be estimated from Doyle's theory.[23] For iron precipitates in MgO this band lies in a far-uv region, at about 7.75 eV, and therefore is shielded by a broad background of the MgO crystal absorption. Still, the presence of metallic aggregates could be inferred from the spectra for samples under discussion, but basing only on the substantial increase in the optical absorption background at short wavelengths (see Fig. 5). This background was found to increase with the increase in the implanted dose and to decrease with the increase in the annealing temperature.

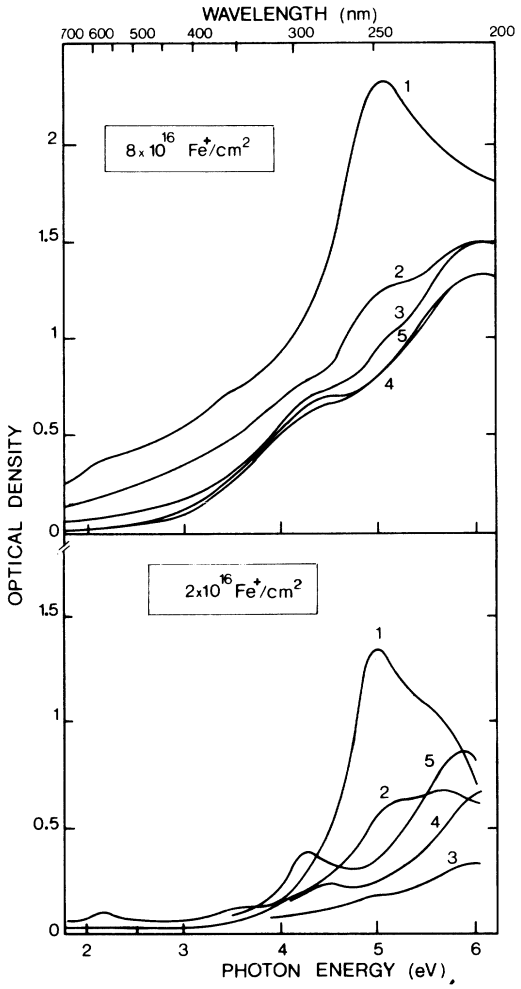

FIG. 5. Optical absorption spectra for MgO crystals implanted with 100-keV $^{56}Fe^+$ ions at doses of 2×10^{16} and 8×10^{16} ions/cm^2 measured for (1) the as-implanted samples and after subsequent annealings in air for 30 min at (2) 600 °C, (3) 700 °C, (4) 800 °C, and (5) 900 °C.

V. CONVERSION-ELECTRON MÖSSBAUER STUDY

Mössbauer spectra were measured using the technique of conversion-electron Mössbauer spectroscopy (CEMS). The experimental methods and applications of CEMS in studies of various materials implanted with ^{57}Fe have been recently reviewed in Ref. 24. Two essential features of CEMS important for this application are the following: (i) CEMS probes only the surface layer of samples, at the depth of about 100 nm, which means a thickness comparable with the implantation range, and (ii) it is mostly insensitive for bulk impurities. The method makes it possible to investigate samples implanted with doses as low as 10^{15} of ^{57}Fe atoms/cm^2, which is hardly measurable with the conventional transmission technique. In the present study the CEMS spectra were measured with the use of two different techniques. The spectra for all low-dose samples ($<10^{16}$ ions/cm^2) were measured with a helium-flow proportional counter in which the sample was placed in backscattering geometry[25] (i.e., the γ-ray incidence an-

gle was 90°). This experimental setup allows for high sensitivity measurements required for the low-dose sample but at room temperature only. All measurements at liquid-nitrogen temperature (and also some measurements at room temperature) were performed using the equipment with channel electron multipliers, as described in Refs. 26 and 27 (the incidence angle was 30° or 45°). The results obtained by different spectra recording systems were practically the same. Sources used for measurements were ^{57}Co in Cr or in Rh matrices, with the activity of about 50–100 mCi. The experimental linewidth was about 0.3 mm s^{-1}. The count rate was typically about 10000 counts s^{-1} in the case of proportional counters and about 1000–2000 counts s^{-1} when using channel electron multipliers. The velocity scale and all the data are referred to a metallic iron absorber at room temperature. Spectra were fitted with the computer least-squares procedure with the assumption of Lorentzian shapes of Mössbauer lines. Some examples of the obtained spectra are presented in Figs. 6, 7, 9, 10, and 12.

A. Dose dependence

Figure 6 presents several Mössbauer spectra measured at room temperature with MgO samples implanted at the energy of 100 keV and doses 3×10^{15}, 2×10^{16}, 4×10^{16}, and 8×10^{16} ions/cm^2. The spectrum of polycrystalline MgO sample implanted with 2×10^{16} ions/cm^2 is included for comparison. A similar set of spectra was obtained also for 70-keV implantations with various doses. Spectra for various samples were also measured at 77 K; two examples are presented in Fig. 7.

The spectra for the as-implanted samples are complex due to a superposition of several overlapping contributions. A consistent decomposition of all the spectra into several components was possible, from which the identification of different charge states of iron in samples under study and their variation with the implantation dose was accomplished. Some of these components could be identified on the basis of the Mössbauer data for samples obtained at equilibrium conditions (either iron[28–31] or cobalt

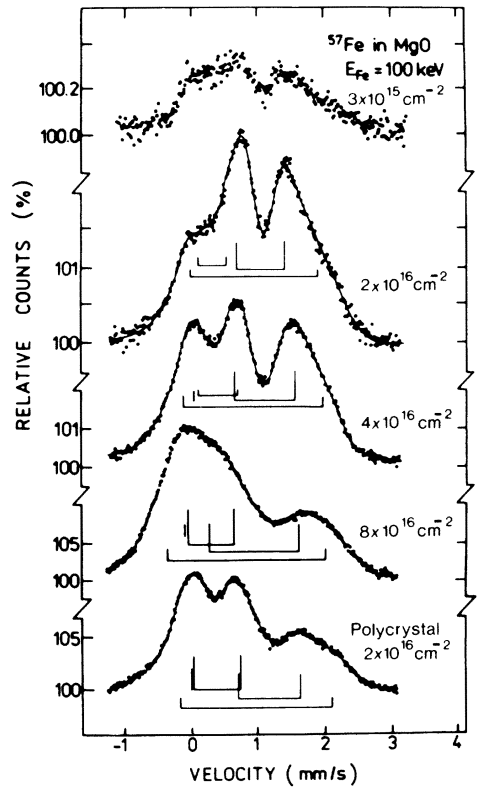

FIG. 6. CEMS spectra at room temperature for MgO crystals implanted with 100-keV $^{57}Fe^+$ ions at doses varying from 3×10^{15} to 8×10^{16} ions/cm^2. Estimated average concentrations for iron per cation are 0.6%, 4%, 8%, and 16%, respectively. For comparison the spectrum obtained with a MgO polycrystalline sample implanted with 100-keV $^{57}Fe^+$ ions at a dose of 2×10^{16} ions/cm^2 is presented at the bottom of the figure.

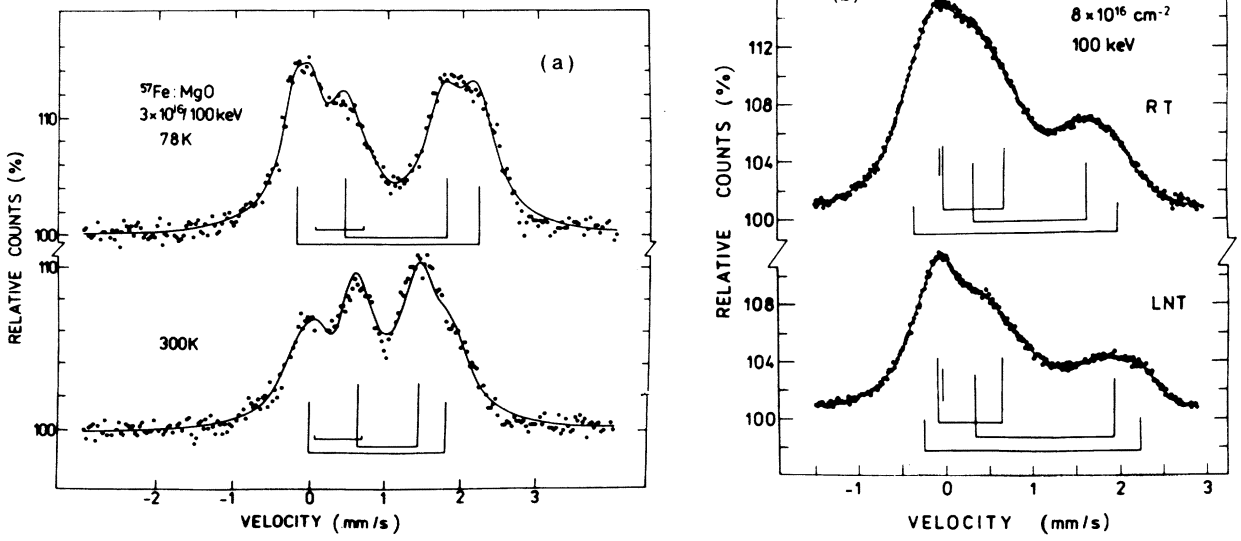

FIG. 7. CEMS spectra for MgO crystals implanted with doses of (a) 3×10^{16} and (b) 8×10^{16} of 100-keV $^{57}Fe^+$ ions/cm^2, measured at 300 and 77 K.

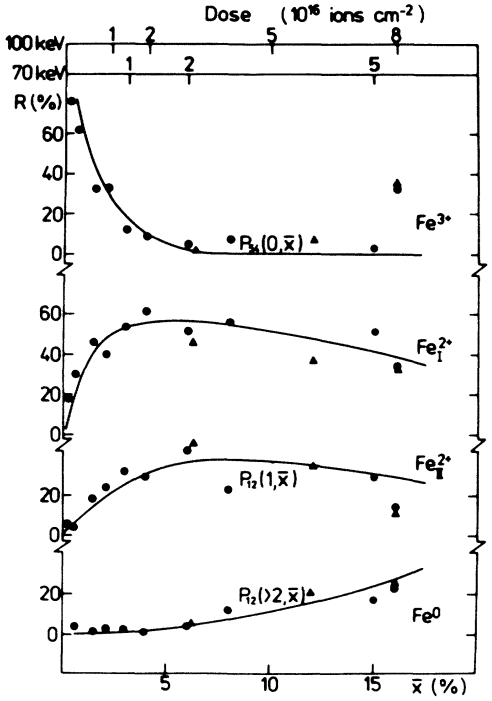

FIG. 8. Fractional contribution of various iron states present in as-implanted Fe-MgO samples (Fe^{3+}, $Fe^{2+}{}_{I}$, $Fe^{2+}{}_{II}$, and metallic iron Fe^{0}), estimated from corresponding components in Mössbauer spectra, and presented vs the concentration of the implanted iron: ● is the room-temperature data and △ is the liquid-nitrogen temperature data. Curves represent the probability functions calculated from the binomial distribution formulas for particular arrangements of iron atoms in MgO lattice [see Sec. VI, Eq. (1)]. $P_{54}(0,\bar{x})$ represents the probability function of finding no other iron atom in the sphere containing 54 cationic sites in MgO. $P_{12}(1,\bar{x})$ and $P_{12}(>2,\bar{x})$ are the probability functions of finding, respectively, 1 and more than 2 iron atoms as nearest-neighbors to iron probe (e.g., in one of the 12 nearest cationic sites).

ions[32] introduced into MgO crystals by a heat treatment). The following components were identified on the basis of the consistent sets of computer fits for all the spectra: Three quadrupole-split doublets and one single line, which can be ascribed, correspondingly, to a ferric iron (Fe^{3+}), two forms of a ferrous iron ($Fe^{2+}{}_{I}$ and $Fe^{2+}{}_{II}$), and to metallic iron (Fe^{0}). The spectra parameters for various components [the isomer shifts (IS), quadrupole splittings (QS), linewidths W, and relative line areas R], obtained from computer fits, are collected in Table I. The values of the isomer shift and the quadrupole splitting for each of the four components are quite constant in the investigated range of concentrations, whereas the relative areas of different components indicate a remarkable concentration dependence, as shown in Fig. 8. The various states identified in the spectra for nonannealed samples have the following properties.

(i) The ferric iron Fe^{3+} is represented by a quadrupole-split doublet with the following parameters: $\Delta_{IS}\simeq 0.4$ mm s^{-1} and $\Delta_{QS}\simeq 0.6$–0.7 mm s^{-1}. These values agree well with the data for Fe^{3+} ions introduced in MgO by classical doping and reported by Wiederisch *et al.*[28] Fe^{3+} is commonly thought to occur in MgO in a form of complexes with vacancies. The contribution of the Fe^{3+} component in the spectra for implanted samples is very substantial for low-dose samples but it is much smaller for high-dose samples: The relative contribution of this fraction is about 60% for 3×10^{15} ions/cm^2 and almost zero at about 3×10^{16} ions/cm^2 (Fig. 8). Thus, the absolute number of Fe^{3+} ions is virtually constant for various samples and does not depend on the implantation dose, while its estimated value (~ 1–2×10^{15} cm^{-2}) corresponds roughly to the number of V-type centers, as determined from optical absorption measurements (~ 1–3×10^{15} cm^{-2}; see Sec. IV). It is remarkable that for a powder sample the relative fraction of the Fe^{3+} species was found to be much higher than that for crystalline species (see Table I, sample nos. 6 and 7), which also indicates that there is a connection of this form of iron with defects.

(ii) Ferrous iron Fe^{2+} is represented by two different quadrupole-split doublets, characterized by the isomer shift $\Delta_{IS}\simeq 1.0$ mm s^{-1}, similar for both doublets, and by two different values of the quadrupole splitting: $\Delta_{QS}\simeq 0.9$–1.1 mm s^{-1} for $Fe^{2+}{}_{I}$ and $\Delta_{QS}\simeq 2.1$–2.3 mm s^{-1} for $Fe^{2+}{}_{II}$ (room-temperature data). Δ_{QS} values for both Fe^{2+} components depend strongly on the temperature of the measurement (see Fig. 7). Both Fe^{2+} fractions increase with the dose at the expense of the Fe^{3+} fraction and reach the values of about 60% ($Fe^{2+}{}_{I}$) and 30% ($Fe^{2+}{}_{II}$) at dose of about 3×10^{16} ions/cm^2 (i.e., $\bar{x}\simeq 6\%$) and then decrease at higher doses (Fig. 8). A comparison of the values of the quadrupole splitting at 300 and 77 K for both $Fe^{2+}{}_{I}$ and $Fe^{2+}{}_{II}$ components indicates that the change in the electric field gradient at low temperature is typical for Fe^{2+} ions in crystalline fields of low symmetry (e.g., for 3×10^{16} ions/cm^2 implanted samples, QS increases from 1.01 to 1.26 mm s^{-1} for $Fe^{2+}{}_{I}$ and from 2.17 to 2.36 mm s^{-1} for $Fe^{2+}{}_{II}$, see Table I and Fig. 7).

(iii) Metallic iron aggregates are represented by a single line located at about 0 mm s^{-1}. The relative contribution of this line increases with the dose, approaching the value of about 20% in high-dose spectra (Fig. 8). It is to be noted that the size of metallic particles in the as-implanted samples is always sufficiently small so that there is no evidence of magnetic hyperfine structure in spectra, both at room temperature and at 77 K. In previous measurements at 4.2 K for a dose of 6×10^{16} ions/cm^2 (Ref. 3) the magnetic pattern was observed and the size of metallic precipitates was estimated as about 2 nm in diameter.

The spectra obtained for the powder sample (no. 7 in Table I and Fig. 6) indicate that in this case, fractions of different iron states present are the same as those observed in monocrystalline samples; however, their relative contributions are different. The relative contributions of various iron states in the powder samples (2×10^{16} ions/cm^2) are comparable with those in the high-dose implanted crystal (no. 12; 8×10^{16} ions/cm^2). The comparability of the high-dose implanted layer of the monocrystal with the polycrystalline sample indicates the role of damage.

B. Annealing behavior

The evolution of Mössbauer spectra with the annealing temperature is presented in Fig. 9 (annealing in air for sample no. 6: 2×10^{16} ions/cm^2, 100 keV) and Fig. 10 (an-

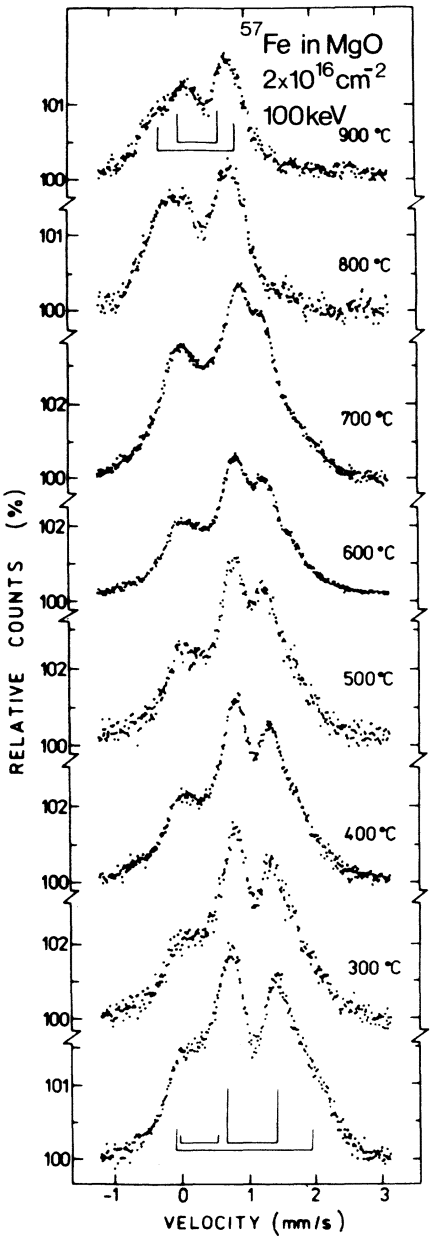

FIG. 9. Evolution of CEMS spectra for an Fe-MgO sample (2×10^{16} ions/cm^2, 100 keV) upon the isochronal annealing (30 min) in air. Measurements were performed at room temperature.

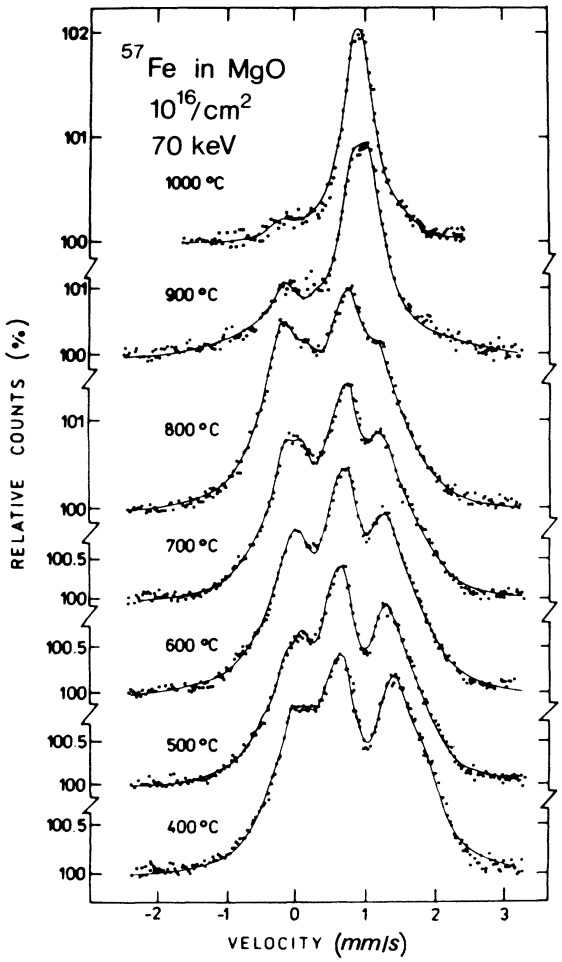

FIG. 10. Evolution of CEMS spectra for an Fe-MgO sample (10^{16} ions/cm^2, 70 keV) upon the isochronal annealing (30 min) in vacuum. Measurements were performed at room temperature.

nealing in vacuum for sample no. 5: 1×10^{16} ions/cm^2, 70 keV). Annealing in air was performed also for sample no. 9 (4×10^{16} ions/cm^2, 100 keV), and a similar behavior was observed as for sample no. 6. A comparison of Mössbauer spectra parameters for annealings in air and in vacuum is given in Fig. 11. The difference in the results for the two annealing procedures can be understood in terms of the Fe^{2+} oxidation and Fe^{3+} kinetics processes studied in Refs. 6 and 18.

As it follows from the data presented in Figs. 9 and 11, the isochronal annealing in air atmosphere causes phenomena that are different in low- ($\lesssim$700 °C) and in high- ($\gtrsim$800 °C) temperature regions. In the first region the states of iron do not change but one observes changes in their relative contributions: A systematic increase in the contribution of the Fe^{3+} fraction and a decrease in the contributions of both the Fe^{2+} and the metallic iron fractions are seen. These changes are accompanied by a slight increase in the value of the quadrupole splitting for the Fe^{3+} state and a decline in the quadrupole splitting value for the Fe^{2+} state (see Fig. 11). After annealing at high temperatures, a transition of all iron states present until 700 °C into a new form of Fe^{3+} is clearly seen. The spectrum presents now an asymmetric pattern which can be decomposed into two quadrupole doublets with the following parameters at room temperature: $\Delta_{IS}=0.35$ mm s^{-1}, $\Delta_{QS}=0.55$ mm s^{-1} and $\Delta_{IS}=0.23$ mm s^{-1}, $\Delta_{QS}=1.2$ mm s^{-1}, respectively. The spectrum corresponds to iron positioned in a structure of spinel, where the octahedral position (Fe_o^{3+}) and the tetrahedral position (Fe_t^{3+}) are occupied. We conclude that, after the high-temperature annealing in air of the sample under study, iron is present in a form of spinel-like precipitates.

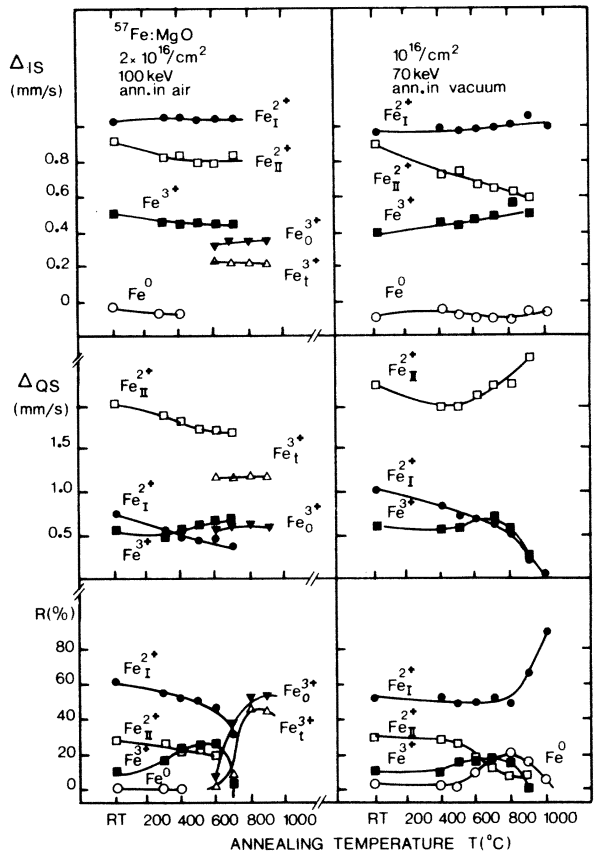

FIG. 11. Comparison of the Mössbauer-spectra parameters for samples annealed in air and in vacuum, in the function of annealing temperature.

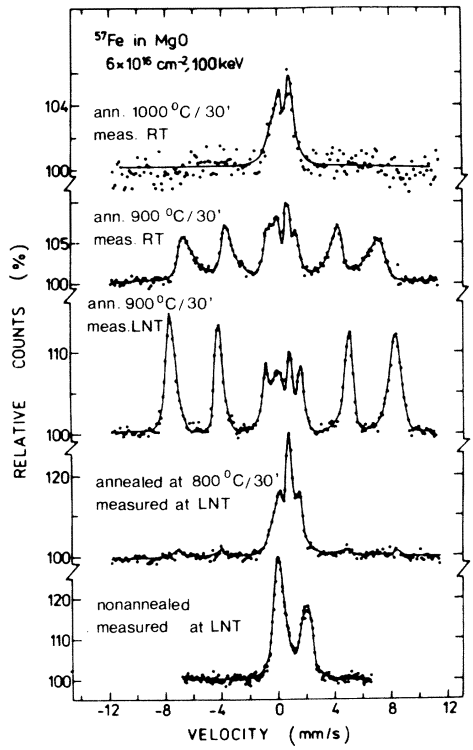

FIG. 12. CEMS spectra for an Fe-MgO sample (6×10^{16} ions/cm^2, 100 keV) indicating the precipitation and growth of superparamagnetic particles of magnesioferrite $MgFe_2O_4$. Annealing temperatures and temperatures of measurements as indicated.

In the case of samples implanted with a high dose of iron (sample no. 10: 6×10^{16} ion/cm^2) and annealed in air at the high-temperature range (>700 °C), the spectra indicate clearly the precipitation of magnesioferrite particles ($MgFe_2O_4$) (Fig. 12). After annealing of the sample at 800 °C these particles are large enough to behave superparamagnetically. The next annealing step (900 °C) results in the size increase: Almost 85% of the iron exists already in a form of magnetic particles of $MgFe_2O_4$. Transmission electron microscopy measurements[4] indicated that the mean size of magnesioferrite particles is about 20 nm in diameter after annealing at 800 °C and 30 nm after 900 °C. After annealing at 1000 °C (Fig. 12) the spectrum has much smaller amplitude, which indicates that iron diffuses out of the region of CEMS measurements ($\simeq$100 nm). The RBS measurements indicated that it was the diffusion towards the surface followed by the evaporation which took place. The process of the growth of magnesioferrite precipitates upon sample annealing was observed for an iron-doped MgO sample by Gonser *et al.*[29] A comparison of the spectra in the two cases indicates that the processes occurring upon sample annealing in both implanted and thermally doped samples are similar.

Annealing in vacuum causes a drastically different effect, resulting, above 800 °C, in a sharp increase of the $Fe^{2+}{}_I$ fraction at the expense of other components (Fig. 11). This process of annealing leads to the formation of a well-dissolved solution of Fe^{2+} in MgO matrix. Such a result is stated on the basis of the spectrum observed (see Fig. 10, top): A single line spectrum is obtained with the isomer shift $\Delta_{IS}\simeq1.0$ mm s^{-1}. Such a spectrum greatly resembles those measured in Refs. 30 and 31 for Fe^{2+} introduced in MgO by means of thermal doping (above 1300 °C) in a reducing atmosphere; the measured spectra were found to be characteristic for Fe^{2+} ions located at substitutional positions in the MgO matrix. Notice that the contribution of the $Fe^{2+}{}_{II}$ fraction decreases with the annealing temperature. It is therefore clear that ferrous ions in this state, which is a less stable state than the $Fe^{2+}{}_I$ state, are not usually observed in MgO samples in which iron impurities were introduced by a high-temperature doping.

VI. DISCUSSION AND CONCLUSIONS

A main characteristic of a high-dose implantation, which defines properties of the implanted layer in ionic crystals, is the presence of both high density of implanted impurities and high density of defects. This induces formation of various impurity-defect complexes and processes of aggregation and precipitation of impurities. A combination of experimental techniques employed in this work allowed us to investigate such phenomena in a complementary way. The CEMS technique allowed us to distinguish different electronic states of implanted iron impuri-

ties and to determine the symmetry of their environments, as well as allowing us to disclose the nature of phases precipitated in MgO matrix both just after the implantation and after the consecutive sample annealing. Optical absorption and ion channeling measurements have given complementary information on the number and characteristics of defects present in the cationic and anionic sublattices of MgO crystals and on their thermal annealing behavior.

In MgO crystals implanted at room temperature at the range of doses 10^{15}–10^{17} ions/cm^2 (average iron concentration from 0.3 to 20 at. %) iron was found to exist in three different states: Fe^{3+}, Fe^{2+}, and metallic precipitates. Relative contributions of these states depend on the implantation dose, as shown in Fig. 8. The fraction of the Fe^{3+} ions is significant only for low-dose implanted samples, and it decreases very quickly with increasing dose. The presence of Fe^{3+} ions in the as-implanted MgO crystals is thought to be correlated with the presence of defects. The number of point defects such as F-, F^+-, and V-type centers in the as-implanted samples increases up to the saturation ($\sim 2\times 10^{21}$ and 3×10^{20} cm^{-3}, respectively) at the dose of about 3×10^{16} ions/cm^2 (Fig. 4). The total number of defects present in the implanted zone must be much larger, which is supported by ion channeling measurements; e.g., for the samples implanted with 2×10^{16} and 3×10^{16} ions/cm^2 the minimum yields measured in the [100] and [110] directions of the Mg sublattice are of the order of 40–60 % (see Fig. 3 and Ref. 3). Also the transmission electron microscopy observations[4] showed a large concentration of extended defects. However, as it results from our TEM and channeling measurements, the MgO matrix is not completely destroyed by iron implantation, and a substantial fraction of iron can be found in well-determined positions, both substitutional and interstitial, in a virtually undestroyed MgO lattice. In addition, the absolute number of V-type centers in the as-implanted samples, which is very comparable with the number of Fe^{3+} ions deduced from Mössbauer measurements [$\sim(1-2)\times 10^{15}$ cm^{-2}], also supports the idea that Fe^{3+} ions exist in the MgO matrix in complexes with defects (cationic vacancies). A connection of the presence of iron in the trivalent state in MgO with lattice defects, observed in implanted samples, agrees with a general observation for samples prepared under thermal conditions: Generally it is accepted that Fe^{3+} ions exist in the MgO matrix, forming complexes with cationic vacancies.[6–8] Recent shell-model calculations of the stability energy of various Fe^{3+}-vacancy complexes performed by Gourdin *et al.*[7] indicate that the $Fe^{3+}O^{2-}VO^{2-}Fe^{3+}$ trimer oriented in the [100] direction is the most stable configuration. Furthermore, it was also found that the tetrahedrally and octahedrally coordinated complex aggregates of solutes and vacancies with oxygen, which form nuclei of mixed oxide-spinel structures, are even more stable and that their stability increases with cluster size. A high stability of these complexes is associated with a large displacement and polarization of the oxygen ion situated between the trivalent ion and the vacancy. Our data for implanted samples indicate the existence of Fe^{3+} in complexes with vacancies, but it is impossible at present to conclude about details of local configurations of the complexes formed.

A strong decrease in the fraction of Fe^{3+} ions with an iron dose can be tentatively explained using a simple statistical model which recently was applied by us for the case of Fe-implanted LiF crystals.[33] In this model, probabilities of finding various iron states for an arbitrary iron concentration $\bar{x}$ are determined by binomial distribution:

$$P_N(n,\bar{x}) = \binom{N}{n} \bar{x}^n (1-\bar{x})^{N-n} , \tag{1}$$

where N corresponds to the number of neighboring atoms which can be substituted by iron and which form complexes of n impurity iron atoms with the iron probe atom. Thus the corresponding probabilities for the presence of an isolated iron ion ($n=0$), iron dimer ($n=1$), trimer ($n=2$), etc., can be evaluated using this formula.

We calculated probability functions from binomial distribution formulas [Eq. (1)] for various arrangements of iron atoms in the MgO lattice, in a function of iron concentration $\bar{x}$. Calculations were performed for probability functions of finding 0, 1, 2, etc., iron atoms [$P(0,\bar{x})$, $P(1,\bar{x})$, $P(2,\bar{x})$, etc., respectively] in the probe vicinity containing only nearest neighbors (P_{12}, twelve Mg atoms) or two, three, and several coordination spheres. Among various probability functions, those which give the best simulation of the experimental data were chosen and were indicated in Fig. 8. A good agreement between the calculated curves and the experimental data indicated, on one hand, that various iron states are strongly related to various and well-determined iron arrangements in the MgO lattice, and on the other hand, it allowed for the identification of these arrangements. It was found that the best simulation of the experimental data is obtained by the following functions. (i) For Fe^{3+}: the $P_{54}(0,\bar{x})$ function, which represents the probability function of finding no other iron atom in the vicinity containing four cationic coordination spheres (54 cationic sites); thus Fe^{3+} represents isolated iron. (ii) For $Fe^{2+}{}_{II}$: the $P_{12}(1,\bar{x})$ function, representing the probability of finding one other iron as a close neighbor (in the first coordination sphere containing 12 cationic sites); thus $Fe^{2+}{}_{II}$ represents iron in dimers. (iii) For Fe^0: the $P_{12}(>2,\bar{x})$ function, representing the probability of finding at least two other iron atoms as close neighbors to the iron probe; thus the Fe^0 state is characteristic for iron clusters of three or more iron atoms. (iv) $Fe^{2+}{}_{I}$ is described by the curve corresponding to all iron configurations other than the three listed above. As seen, different valence states of iron implanted in a MgO matrix correspond to distinctly different local configurations of iron impurities. The statistical model employed for the case of Fe implanted in LiF crystals also allowed for the assignment of various states of iron to specific configurations of iron.[33] In this case the Fe^{3+} concentration dependence was well reproduced by the $P_{12}(0,\bar{x})$ probability, which indicates that iron may remain in a Fe^{3+} state in LiF as long as there is no other iron ion at a nearest-neighbor cationic site. For the MgO-Fe system, the experimentally observed variation of the number of Fe^{3+} ions with iron concentration occurs more quickly than the decrease of the probability function $P_{12}(0,\bar{x})$. As seen in Fig. 8, the probability $P_{54}(0,\bar{x})$ fits the dependence of the Fe^{3+} fraction in MgO on iron concentration very well. One concludes that Fe^{3+} in MgO can exist only as an isolated impurity so that the presence

of another iron impurity in a distance closer than four cationic coordination spheres causes the change of the valence state of the iron ion, either into Fe^{2+} or Fe^0. It is worth noticing that the exclusion volume around the Fe^{3+} ion as found from our model ($N=54$ cationic sites) is characteristic for the complexes of Fe^{3+}-vacancy-Fe^{3+}, proposed by Gourdin *et al.*[7] and discussed above. Therefore our result may be perhaps an indication that Fe^{3+} in MgO exists in Fe^{3+}-vacancy complexes of the Gourdin type.

A characteristic feature of the as-implanted MgO-Fe systems, in the range of iron concentrations investigated, is a high fraction of Fe^{2+} ions. The total Fe^{2+} fraction is distributed over two different sites, $Fe^{2+}{}_{I}$ and $Fe^{2+}{}_{II}$, characterized by the same value of the isomer shift ($\Delta_{IS}\simeq 1.0$ mm s^{-1}) in the Mössbauer spectra but by two different values of the quadrupole splitting ($\Delta_{QS}\simeq 0.9$–1.1 mm s^{-1} and $\Delta_{QS}\simeq 2.1$–2.3 mm s^{-1}). Both Fe^{2+} fractions increase very sharply in a low-dose region ($<3\times10^{16}$ ions/cm^2), but the dose dependence of the two is different (see Fig. 8). The Mössbauer pattern for the $Fe^{2+}{}_{I}$ component is quite comparable to that for the magnesio-wüstite solid solution $Mg_{1-x}Fe_xO$, which corresponds to a random distribution of Fe^{2+} ions in MgO matrix. According to the equilibrium phase diagrams for the MgO-Fe system,[9,10] the magnesio-wüstite is stable at high temperature, but it decomposes to the mixture of magnesioferrite and magnesio-wüstite during a slow cooling. In implanted systems the magnesio-wüstite solution is created without the precipitation of sizable magnesioferrite particles. A good solubility of Fe^{2+} in MgO matrix is facilitated by a small size mismatch between the Fe^{2+} and Mg^{2+} ions (0.76 and 0.65 Å, respectively). Also the lattice parameter of wüstite is only slightly different from that of the MgO ($a_{FeO}=4.307$ Å, $a_{MgO}=4.213$ Å). For the magnesio-wüstite compounds the lattice parameter takes a value between those for pure FeO and MgO and depends on the composition (e.g., $a=4.225$ Å in $Fe_{0.1}Mg_{0.9}O$ and $a=4.298$ Å in $Fe_{0.75}Mg_{0.25}O$). The Mössbauer spectra for magnesio-wüstite are known from the literature, e.g., Refs. 34 and 35. A well-defined quadrupole splitting was observed for $Fe_{1-x}O$ and also for series of solid solutions $Mg_{1-x}F_xO$. The magnitude of the quadrupole splitting is known to increase with the concentration of iron [in particular, for $Mg_{0.9}Fe_{0.1}O$, $\Delta_{QS}\simeq 0.7$–0.8 mm s^{-1} (Ref. 35)] and with the number of lattice defects in magnesio-wüstite. The magnitude of the isomer shift $\Delta_{IS}\simeq 1.0$–1.1 mm s^{-1} in magnesio-wüstite is in good agreement with our results for the $Fe^{2+}{}_{I}$ component.

It is worth noting that in conventionally doped MgO crystals[30,32] the divalent iron is a main fraction with the Mössbauer parameters as for our $Fe^{2+}{}_{I}$ fraction. The $Fe^{2+}{}_{II}$ fraction seems to be specific for implanted systems. A metastability of the $Fe^{2+}{}_{II}$ component is clearly shown by changes in the spectra measured after consecutive steps of annealing in vacuum: The $Fe^{2+}{}_{I}$ component increases very sharply above 800 °C and mostly at the expense of the $Fe^{2+}{}_{II}$ component (see Fig. 11). As it results from the analysis of the dose dependence for $Fe^{2+}{}_{II}$ in the statistical model (Fig. 8), the $Fe^{2+}{}_{II}$ state of iron is formed when iron exists in the MgO matrix in the form of dimers aligned in the [110] direction.

It is notable that the statistical model also accounts for the concentration dependence of the metallic aggregate component deduced from Mössbauer data (Fig. 8). In this case the probability of aggregating three or more iron atoms in the nearest-neighbor cationic sites gives a good description of the concentration dependence of the metallic iron component. These small iron aggregates could be the nucleation centers for metallic iron precipitation.

The presence of the large Fe^{2+} fraction in the as-implanted MgO crystals is responsible for a dramatic electrical conductivity modification in this material. As it was observed[5] this modification consists in an insulator-conductor transition around the threshold dose of 3×10^{16} Fe ions/cm^2 (i.e., $\bar{x}\simeq 6\%$). Above this dose, the conductivity increases rapidly to the value of $\sim 100\ \Omega^{-1}\,\mathrm{cm}^{-1}$ at 10^{17} ions/cm^2. This effect can be explained assuming that Fe^{2+} ions act as electron hopping centers. Our interpretation discussed above for the distribution of Fe^{2+} ions is consistent with this assumption.

Annealing phenomena presented in Sec. V can be discussed in two temperature regions: first, below 700 °C and the second between 700 and 1000 °C. Annealing in the first temperature range is connected with several correlated phenomena observed by the three techniques of investigations employed. CEMS measurements show continuous process of oxidation of Fe^{2+} to Fe^{3+}, which is accompanied by some changes in the local symmetry as indicated by the increase of the Δ_{QS} value for this component (Fig. 11) as well as an increase in the minimum yield χ_{min} for Fe measured in both [100] and [110] channels (Fig. 3). At the same time, no significant rearrangement is observed in the magnesium sublattice (Fig. 3), but optical absorption measurements show a complete annealing of V-type and F-type centers (Fig. 5). It is remarkable that the same behavior of the Fe^{3+} fraction is also observed from CEMS spectra measured with samples annealed in vacuum (Fig. 11). This could indicate that the oxidation processes in this low-temperature range occur without external oxygen. In this case the oxidation of Fe^{2+} can take place subsequently to the migration of V^--type centers (Mg^{2+} vacancy with a trapped hole) and their combination with Fe^{2+} ions. Fe^{3+} ions formed by this mechanism are characterized by the same Δ_{IS} value ($\simeq 0.40$ mm s^{-1}) as measured for Fe^{3+} ions in as-implanted samples. Thus the formation of the same kind of Fe^{3+}-vacancy complexes can be considered. In the high-temperature range (800–1000 °C), annealing processes in air and in vacuum are drastically different. In the case of annealing in air one observes the transformation of iron into two new ferric ion states: $Fe_o{}^{3+}$ and $Fe_t{}^{3+}$ (Fig. 11). As suggested in Sec. V these two states correspond to Fe^{3+} ions, respectively, in octahedral and tetrahedral sites. This new arrangement of iron ions is accompanied by a quasicomplete restoration of the magnesium sublattice, as reported by channeling study (Fig. 3), and diffusion of iron as shown by the profile broadening (Fig. 1). This is in agreement with the formation of magnesioferrite precipitates identified in high-dose implanted samples annealed in air in the high-temperature range (e.g., 6×10^{16} ions/cm^2, Fig. 12). In the case of low-dose implanted samples (e.g., 2×10^{16} ions/cm^2, Fig. 9) the spinel-like aggregates are still too small (<5 nm) to display hyperfine structure in Mössbauer spectra measured at 300 and 77 K (Ref. 29). We must note that the magnesioferrite structure fits the

MgO structure very well. Magnesioferrite $MgFe_2O_4$ is a nominally inverse spinel in which O^{2-} ions form the same fcc closed-packed structure as in MgO while iron is occupying almost equally tetrahedral and octahedral sites. The presence of such precipitates has been confirmed by our previous transmission electron microscopy observation on implanted Fe-MgO specimens.[4] It was shown that the $MgFe_2O_4$ precipitates are in epitaxy with the MgO matrix and their orientation relationship is the following: $(001)_{spinel}||(001)_{MgO}$ and $[100]_{spinel}||[100]_{MgO}$. The small coherent precipitates of magnesioferrite may also grow in MgO crystals doped with iron upon heat treatment in air already at 700–800 °C.[10–12,16] Therefore the precipitation of magnesioferrite particles in implanted samples after annealing at 800 °C in air is well substantiated by the classical thermodynamic properties of the Fe-MgO system.

In contrast, annealing in vacuum at temperatures higher than 800 °C converts all iron to $Fe^{2+}{}_I$ components, which is accompanied by a gradual decrease of the Δ_{QS} value down to zero at 1000 °C. This is explained by total reduction of iron and dilution in the MgO matrix. The same behavior has been observed in Fe-doped MgO crystals thermally treated in reducing atmosphere.[30,31] Thus by comparing the annealing behavior in air and in vacuum one concludes that oxygen pressure plays a significant role, mostly in the high-temperature range, compared to the low-temperature range (< 700 °C) in which internal processes associated with lattice defects seem predominant. In the case of annealing in air in the high-temperature range the oxidation mechanism proposed by Groves and Fine[10] can be considered. In this mechanism, oxygen atoms, by adding on the surface of the crystal, create cationic vacancies and holes which diffuse together in the crystal and oxidize Fe^{2+} ions in the interior.

[1]D. A. Thomson, Radiat. Eff. 56, 105 (1981).

[2]A. Perez, M. Treilleux, P. Thevenard, G. Abouchacra, G. Marest, L. Fritsch and J. Serughetti, in *Metastable Materials Formation by Ion Implantation,* edited by S. T. Picraux and W. J. Choyke, Materials Research Society Symposia Proceedings (North-Holland, New York, 1982), Vol. 7, pp. 159–166.

[3]A. Perez, J. P. Dupin, O. Massenet, G. Marest, and P. Bussière, Radiat. Eff. 52, 127 (1980).

[4]A. Perez, M. Treilleux, L. Fritsch, and G. Marest, Nucl. Instrum. Methods 182-183, 747 (1981).

[5]A. Perez, J. Bert, G. Marest, B. D. Sawicka, and J. A. Sawicki, in Proceedings of the International Conference on Ion Beam Modification of Materials, Grenoble, France, 1982 [Nucl. Instrum. Methods (in press)].

[6]R. A. Weeks, J. Gastineau, and E. Sonder, Phys. Status Solidi A 61, 265 (1980).

[7]W. H. Gourdin and W. D. Kingery, J. Mater. Sci. 14, 2053 (1979).

[8]W. H. Gourdin, W. D. Kingery, and J. M. Driear, J. Mater. Sci. 14, 2074 (1979).

[9]B. Phillips, S. Somiya, and A. Muan, J. Amer. Chem. Soc. 44, 167 (1961).

[10]G. E. Groves and M. E. Fine, J. Appl. Phys. 35, 3587 (1964).

[11]G. P. Wirtz and M. E. Fine, J. Appl. Phys. 38, 3729 (1967); J. Amer. Chem. Soc. 51, 402 (1968).

[12]K. N. Woods and M. E. Fine, J. Amer. Chem. Soc. 52, 186 (1969).

[13]P. Hing and G. W. Groves, J. Mater. Sci. 7, 422 (1972).

[14]A. S. Kunsetsov and I. V. Yaek, Fiz. Tverd. Tela (Leningrad) 18, 3522 (1976) [Sov. Phys.—Solid State 18, 2051 (1976)].

[15]F. A. Modine, E. Sonder, and R. A. Weeks, J. Appl. Phys. 48, 3514 (1977).

[16]R. S. de Biasi and T. C. Devezas, J. Appl. Phys. 49, 2466 (1978).

[17]L. E. Halliburton and L. A. Kappers, Solid State Commun. 26, 111 (1978).

[18]E. Sonder, T. G. Stratton, and R. A. Weeks, J. Chem. Phys. 70, 4603 (1979).

[19]D. O. Connell, B. Henderson, and J. M. Bolten, Solid State Commun. 38, 283 (1981).

[20]G. Dearnaley, J. H. Freeman, R. S. Nelson, and J. Stephen, in *Ion Implantation, Series Defects in Crystalline Solids,* edited by S. Amelinckx, R. Gevers, and J. Nihoul (North-Holland, Amsterdam, 1973), Vol. 8.

[21]We are indebted to Professor R. Bador from the Laboratoire de Biophysique for his assistance in x-ray spectrometry measurements.

[22]E. Sonder and W. A. Sibley, in *Point Defects in Solids,* edited by J. H. Crawford and L. M. Slifkin (Plenum, New York, 1972), Vol. 1, pp. 201–290.

[23]W. T. Doyle, Phys. Rev. 111, 1067 (1958).

[24]B. D. Sawicka and J. A. Sawicki, in *Topics in Current Physics,* edited by U. Gonser (Springer, Berlin, 1981), Vol. 25, pp. 139–166.

[25]J. Stanek, J. A. Sawicki, and B. D. Sawicka, Nucl. Instrum. Methods 130, 613 (1975).

[26]O. Massenet, Nucl. Instrum. Methods 153, 419 (1978).

[27]J. A. Sawicki, T. Tyliszczak, and O. Gzowski, Nucl. Instrum. Methods 190, 433 (1981).

[28]H. Wiederisch, U. Gonser, R. W. Grant, and A. H. Muir, Bull. Am. Phys. Soc. 10, 709 (1965).

[29]U. Gonser, H. Wiederisch, and R. W. Grant, J. Appl. Phys. 39, 1004 (1968).

[30]D. J. Simkin, P. J. Ficalora, and R. A. Bernheim, Phys. Lett. 19, 536 (1965).

[31]H. R. Leider and D. N. Pipkorn, Phys. Rev. 165, 494 (1968).

[32]J. Chappert, R. B. Frankel, A. Miseitich, and N. A. Blum, Phys. Rev. 179, 578 (1969).

[33]J. Kowalski, G. Marest, A. Perez, B. D. Sawicka, J. A. Sawicki, J. Stanek, and T. Tyliszczak, in Proceedings of the International Conference on Ion Beam Modification of Materials, Grenoble, France, 1982 [Nucl. Instrum. Methods (in press)].

[34]U. A. Kozheurov, U. U. Mikhailov, A. A. Zhukovitskii, B. S. Bokstein, A. A. Lykasov, Ju. S. Kuznetsov, S. Ju. Gurievith, and S. S. Nikolskii, Sov. J. Phys. Chem. 46, 2246 (1972).

[35]G. Shirane, D. E. Cox, and S. L. Ruby, Phys. Rev 125, 1158 (1962).